Hidden order in crackling noise during peeling of an adhesive tape

Jagadish Kumar,[1] M. Ciccotti,[2] and G. Ananthakrishna[1]

[1]*Materials Research Centre, Indian Institute of Science, Bangalore 560012, India*

[2]*Laboratoire des Colloïdes Verres et Nanomatériaux, CNRS UMR 5587, Université de Montpellier II, Place Bataillon,*

34095 Montpellier CEDEX 5, France

We address the longstanding problem of recovering dynamical information from noisy acoustic emission signals arising from peeling of an adhesive tape subject to constant traction velocity. Using the phase space reconstruction procedure we demonstrate the deterministic chaotic dynamics by establishing the existence of correlation dimension as also a positive Lyapunov exponent in a midrange of traction velocities. The results are explained on the basis of the model that also emphasizes the deterministic origin of acoustic emission by clarifying its connection to stick-slip dynamics.

Adhesion continues to generate new directions of interest due to the wide ranging interdisciplinary issues involved and its technological importance. For instance, the recent surge in interest can be traced to its relevance to biological systems, in particular, the desire to design adhesive materials that mimic fibrillar adhesion inherent to biological species such as the gecko [1]. Despite the progress, day-to-day experience like acoustic emission (AE) during peeling of an adhesive tape has remained ill explained. This can be traced to the fact that most information is obtained from quasistatic or near steady state conditions, and much less attention has been paid to nonequilibrium time dependent dissipative aspects of adhesion, and related phenomena such as friction (which is adhesion and wear) [2–4] as also AE. As kinetic and dynamical aspects involve the interplay of internal relaxation time scales (determined by molecular mechanisms) with the applied time scale, they are important in a variety of situations that are subject to fluctuating forces such as flexible joints, composites, and even dynamics of cell orientation [5].

Dynamical information can be obtained using experiments on peeling of an adhesive tape mounted on a roller. These experiments show that peeling is jerky accompanied by a characteristic crackling noise [6,7]. The jerky nature is attributed to the switching of the peel process between two stable dissipative branches separated by an unstable one. (The low and high velocity branches arise from viscous dissipation and brittle fracture, respectively.) The negative force-velocity relation is common to many stick-slip situations, for example, sliding friction [3,4] and the Portevin-Le Chatelier (PLC) effect, a plastic instability observed in tensile deformation of dilute alloys [8], to name only two. In general, stick-slip dynamics results from a competition among inherent time scales [8,9], here, the viscoelastic time scale and the time scale of the pull speed. All stick-slip processes are examples of deterministic nonlinear dynamics.

In contrast to the stick-slip nature of peeling, the origin of AE (even in the general context) is ill understood. Recently, we suggested that the energy dissipated in the form of AE can be modeled in terms of the local displacement rate [10]. A model relevant for the experimental setup that includes such a term reproduces major experimental features of AE as also that of the peel front dynamics [10]. The model also predicts spatiotemporal chaos for a specific set of param-eters. Moreover, it is long believed that AE and stick-slip peel dynamics are related. But, establishing such a connection requires extracting quantitative dynamical information from the AE signals which so far has not been possible, largely due to the highly noisy nature of AE signals. Here, we show that deterministic dynamics governs the AE process by demonstrating the existence of chaotic dynamics using nonlinear time series analysis. The results are explained using a model that also provides insight into the connection between AE signals and stick-slip dynamics.

Retrieval of information about the underlying process is also important in the general context of AE as it is observed in a large number of systems such as the microfracturing process, volcanic activity [11], collective dislocation motion [12,13], etc. However, most studies [11,12], except Ref. [13], are simple statistical studies showing the power law distribution of AE signals as experimental realizations of self-organized criticality [14]. Even in Ref. [13], the extracted fractal dynamics of dislocation generated AE sources is aided by use of multiple transducers. However, the situation is more complex in peeling experiments as only a single transducer is used leading to scalar AE signals that are also substantially noisy, making the intended task even more challenging.

To verify the prediction of chaotic dynamics, we have performed peeling experiments of an adhesive tape mounted on a roller driven at a constant traction velocity in the wide range 0.2 to 7.6 cm/s. A schematic of the experimental setup is shown in Fig. 1(a). An adhesive roller tape of radius R is mounted on an axis passing through O with a motor positioned at O' that provides a constant pull speed V. AE signals associated with stick-slip dynamics are monitored using a high quality microphone. Signals were digitized at the stan-
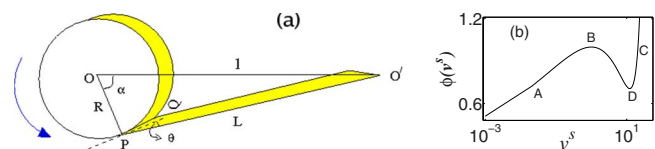

FIG. 1. (Color online) (a) A schematic of the experimental setup. (b) Plot of the scaled peel force function $\phi(v^s)$ as a function of v^s.
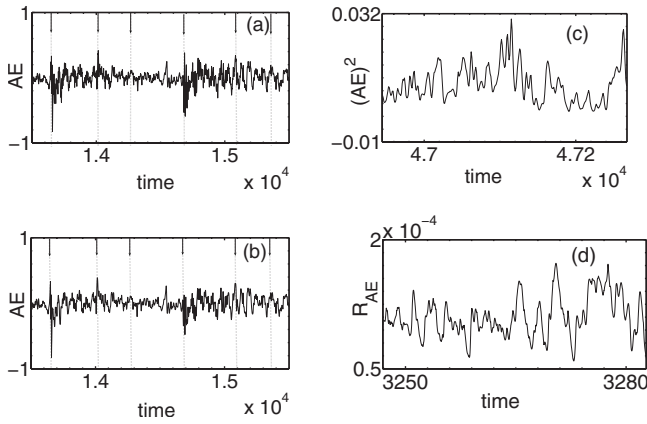
FIG. 2. (a) Raw and (b) cured AE signal for $V=4.8$ cm/s. (c) Square of the amplitude (in arbitrary units) for the data in (b). (d) model AE signal for $V^s=2.48$ and $m=0.001$ which is similar to (c) except for the magnitude of fluctuations.
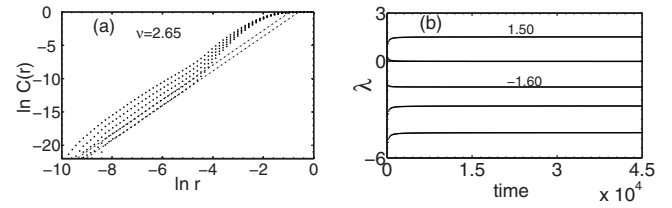

FIG. 3. (a) Correlation integral for pull velocity 4.8 cm/s from $d=6$ to 10. Dashed lines are guides for the eye. (b) Lyapunov spectrum of the AE signals for traction velocities $V=4.8$ cm/s.

dard audio sampling frequency of 44.1 kHz (having 6 kHz band width) with 16 bit signals stored in raw binary files. For low pull speeds V, regular AE bursts are seen that correspond to stick-slip events separated by an oscillatory decaying amplitude. With increasing pull velocity, the AE bursts become irregular and continuous, as shown in Fig. 2(a). There are 38 data files, each containing 1.2×10^6 points. As in most experiments on AE, signals are noisy.

Time series analysis (TSA) begins by unfolding the dynamics through phase space reconstruction of the attractor by embedding the time series in a higher dimensional space using a suitable time delay [15]. Let $[x(k),\ k=1,2,3,\dots,N]$ be the AE signal with Δt as the sampling time. Then, d-dimensional vectors are defined by $\vec{\xi}_k = [x(k),x(k+\tau),\dots,x(k+(d-1)\tau)];$ $\quad k=1,\dots,[N-(d-1)\tau]$. The delay time τ is obtained either from the autocorrelation function or mutual information [16]. Then, the chaotic nature of the attractor is quantified by establishing the existence of correlation dimension and a positive Lyapunov exponent.

The correlation integral defined as the fraction of pairs of points $\vec{\xi}_i$ and $\vec{\xi}_j$ whose distance is less than r, is given by $C(r) = \frac{1}{N_p}\Sigma_{i,j}\Theta(r-|\vec{\xi}_i-\vec{\xi}_j|)$, where $\Theta(\cdots)$ is the step function and N_p the number of vector pairs summed. A window is imposed to exclude temporally correlated points [16]. If the attractor is self-similar, then $C(r) \sim r^\nu$, where ν is the correlation dimension [15]. Then, as d is increased, one expects to find convergence of the slope $dlnC(r)/dlnr$ to a finite value in the limit of small r. In practice, the scaling regime is found at intermediate length scales due to the presence of noise.

As the AE signals are noisy, we have used a modified Eckmann's algorithm suitable for noisy time series [17]. Briefly, Eckmann's algorithm [18] relies on connecting the initial small difference vector $\vec{\xi}_i-\vec{\xi}_j$ to an evolved difference vector through a set of tangent matrices. The number of neighbors used is typically min$[2d,d+4]$ contained in shell size ϵ_s defined by inner and outer radii ϵ_i and ϵ_0, respectively (ϵ_i also acts as a noise filter). The modification we effect is to allow a larger number of neighbors so that the noise statistics

superposed on the signal is sampled properly. We impose an additional constraint that the sum of the exponents be negative for a dissipative system, and also demand the existence of stable positive and zero exponents (a necessary requirement for continuous time systems like AE) over a finite range of shell sizes ϵ_s. The algorithm works well for reasonably high levels of noise in model systems [17] as also for experimental time series (for details, see Ref. [17]). We have also repeated the analysis using the TISEAN package [16].

The data sets are first cured using a noise reduction technique [16]. Figures 2(a) and 2(b) show the raw and cured data, respectively, for $V=4.8$ cm/s. Clearly, the dominant features (the peaks shown by arrows) of the time series are retained except that the amplitude is reduced [16]. Indeed, the two stage power law distribution for the amplitude of AE signals for the raw data are retained except that the exponent for small amplitudes is reduced (from 0.33 to 0.24) without altering that for the large amplitudes. The cured data are used to calculate the correlation dimension for all the data files. However, while raw data are adequate for calculating the Lyapunov spectrum from our algorithm, cured data are required for the TISEAN package. To reduce the computational time, only one fifth of the total points are used.

The autocorrelation time is 4 units in sampling time. A smaller value of $\tau=1$ is used to calculate $C(r)$. A log-log plot of $C(r)$ for the pull velocity 4.8 cm/s is shown in Fig. 3(a) for $d=6$ to 10. A scaling regime of three orders of magnitude is seen with $\nu \sim 2.65 \pm 0.05$. However, converged values of ν (using our method and TISEAN package) are seen, only for data sets for pull velocities from 3.8 to 6.2 cm/s with ν in the range 2.6 to 2.85 ± 0.05.

Using our algorithm, the calculated Lyapunov spectrum is shown in Fig. 3(b) for $V=4.8$ cm/s keeping $\epsilon_o=0.065$. Note that the second exponent is close to zero as expected of continuous flow systems. We have calculated Lyapunov spectrum for the full range of traction velocities and we find (stable) positive and zero exponents [19] only in the region 3.8 to 6.2 cm/s, consistent with the range of converged values of ν.

As a cross check, we have calculated the Kaplan-Yorke dimension D_{ky} from the relation $D_{ky}=j+\frac{\Sigma_{i=1}^{j}\lambda_i}{|\lambda_{j+1}|}$; $\Sigma_{i=1}^{j}\lambda_i > 0$; $\Sigma_{i=1}^{j+1}\lambda_i < 0$. For the case shown in Fig. 3(b), we find $D_{ky}=2+1.5/1.6=2.94$ consistent with ν obtained from $C(r)$ [19]. Similar deviations are seen for other pull velocities. The D_{ky} values obtained from the TISEAN package are uniformly closer to the ν values, typically $D_{ky}=\nu+0.1$. Finally, we note that the positive exponent decreases toward the end of the chaotic domain (6.2 cm/s). These results show unam-

biguously that the underlying dynamics responsible for AE during peeling is chaotic in a midrange of pull speeds.

To understand the results, consider a recent model for peeling of an adhesive tape [10]. In Fig. 1(a), the distance OO' is denoted by l and the peeled length of the tape PO' by L. The angle between the tangent to the contact point P (projection of the contact line PQ onto the plane of the paper) and PO' is denoted by θ and the angle $\angle POO'$ by α. From Fig. 1(a), we get $L \cos \theta = -l \sin \alpha$ and $L \sin \theta = l \cos \alpha - R$. As the peel point P moves with a local velocity v, the pull velocity is given by $V = v + \dot{u} + R \cos \theta \, \dot{\alpha}$. Defining $u(y)$ to be the displacement with respect to the uniform "stuck" peel front and defining $v(y), \theta(y)$, and $\alpha(y)$ at all points y along the contact line, the above equation generalizes to

$$\frac{1}{b}\int_0^b [V - v(y) - \dot{u}(y) - R\dot{\alpha}(y)\cos \theta(y)]dy = 0, \qquad (1)$$

where b is the width of the tape. As the contact line dynamics is controlled by the soft glue, we assume that the effective elastic constant k_g along the contact line is much smaller than that of the tape material k_t. This implies that the force along PO' equilibrates fast and the integrand in Eq. (1) can be assumed to vanish for all y.

The basic idea of the model is that while stick-slip dynamics is controlled by the peel force function $f(v)$, the associated AE is the energy dissipated during rapid movement of the peel front. We begin by defining dimensionless variable $\tau = \omega_u t$, with $\omega_u^2 = (k_t/b\rho)$ where ρ is the mass per unit width of the length L. Similarly, we define $u = Xd$, $l = l^s d$, $L = L^s d$, and $R = R^s d$ using a basic length scale $d = f_{max}/k_t$, where $f_{max} = f(v_{max})$ is the maximum value of the peel force function $f(v)$. We define the scaled peel force function by $\phi(v^s) = f(v^s(v))/f_{max}$ [Fig. 1(b)]. Here, $v^s = v/v_c \omega_u d$ and $V^s = V/v_c \omega_u d$ are the dimensionless peel and pull velocities, respectively, with $v_c = v_{max}/\omega_u d$. Using a scaled variable $r = y/a$, with a referring to a unit length along the peel front, the scaled kinetic energy can be written as $U_K^s = \frac{1}{2C_f}\int_0^{b/a}[\dot{\alpha}(r) + \frac{v_c v^s(r)}{R^s}]^2 dr + \frac{1}{2}\int_0^{b/a}[\dot{X}(r)]^2 dr$. Here the first term represents the rotational kinetic energy and the second term the kinetic energy of stretched tape. $C_f = (f_{max}/k_t)^2(\rho/\xi)$ represents the relative strength of the two terms, where ξ is the moment of inertia per unit width of the roller tape. The potential energy is given by $U_P^s = \frac{1}{2}\int_0^{b/a}X^2(r)dr + \frac{k_0}{2}\int_0^{b/a}[\frac{\partial X(r)}{\partial r}]^2 dr$ with $k_0 = (k_g b^2/k_t a^2)$. The first term arises from the displacement of the peel front due to stretching of the tape and the second term due to inhomogeneity along the front. The total dissipation is the sum of dissipation arising from the peel force function $\phi(v^s)$ and from the rapid movement of the peel front given by $\mathcal{R}^s = \frac{1}{b}\int_0^{b/a}\int \phi(v^s(r))dv^s dr + \frac{1}{2}\int_0^{b/a}\gamma_u[\frac{\partial X(r)}{\partial r}]^2 dr$, respectively. $\phi^s(v^s)$ is assumed to be derivable from a potential function $\Phi(v^s) = \int \phi(v^s)dv^s$. The second term denoted by R_{AE} is the Rayleigh dissipation functional which is interpreted as the energy dissipated in the form of AE. The scaled γ_u is related to the unscaled dissipation coefficient Γ_u through $\gamma_u = \Gamma_u \omega_u/(k_t a^2)$.
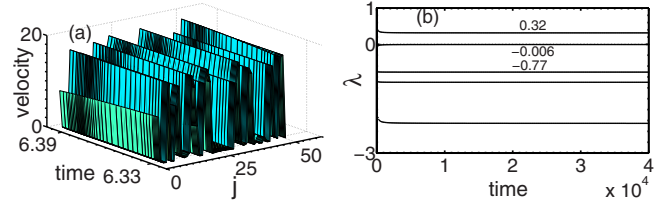

FIG. 4. (Color online) (a) Stuck-peeled configuration for $V^s = 2.48$ and $m = 0.001$. (b) The corresponding Lyapunov spectrum for R_{AE}.

The scaled local form of Eq. (1) is

$$\dot{X} = (V^s - v^s)v_c + R^s\frac{l^s}{L^s}(\sin \alpha)\dot{\alpha}. \qquad (2)$$

Using Lagrange equations of motion, we obtain

$$\ddot{X} = -X + k_0\frac{\partial^2 X}{\partial r^2} + \frac{\phi(v^s)}{(1 + l^s/L^s \sin \alpha)} + \gamma_u\frac{\partial^2 \dot{X}}{\partial r^2}, \qquad (3)$$

$$v_c\dot{v}^s = \frac{R^s l^s}{L^s}\left\{ \dot{\alpha}^2\left[\cos \alpha - R^s l^s\left(\frac{\sin \alpha}{L^s}\right)^2\right] + \ddot{\alpha}\sin \alpha \right\} - \ddot{X}, \qquad (4)$$

$$\ddot{\alpha} = -\frac{v_c\ddot{v}^s}{R^s} - C_f R^s\frac{l^s/L^s \sin \alpha}{(1 + l^s/L^s \sin \alpha)}\phi(v^s). \qquad (5)$$

Equations (2)–(5) are solved using an adaptive step size stiff differential equations solver (MATLAB "ode15s") with open boundary conditions. The nature of the dynamics depends on the pull velocity V^s, the dissipation coefficient γ_u, and C_f. C_f depends on the roller inertia $I = \xi b$ ($10^{-5} \leq I \leq 10^{-2}$) and the tape mass $m = \rho b$ ($0.001 \leq m \leq 0.1$). γ_u ranges from 0.001 to 0.1. Other parameters are fixed at $R^s = 0.35$, $l^s = 3.5$, $k_0 = 0.1$ ($k_t = 1000$ N/m), and $N = 50$. The (unscaled) peel force function $f(v)$ preserves major experimental features like the values of f_{max}, v_{max}, and the velocity jump [6].

The results reported are for $m = 0.001$, and 0.055, $I = 0.01$ and low dissipation coefficient $\gamma_u = 0.01$. Physically, low γ_u implies weak coupling between velocities on neighboring points on the peel front. Thus, local dynamics dominates and hence more ruggedness leading to higher dissipation R_{AE} (than for large γ_u). Indeed, even for low V^s, the peel front breaks up into stuck and peeled segments [see Fig. 4(a) for $V^s = 2.48$ and also Ref. [10]]. Hence, the acoustic energy dissipated R_{AE} is noisy.

Several qualitative features of the experimental AE signals such as the change from burst to continuous type with pull velocity are displayed by R_{AE}. The observed two stage power law distribution for the experimental AE signals is reproduced by the model. For instance, for the model signal in Fig. 2(d), the exponent values are $m_E = 0.6$ and 2.0 for small and large values, respectively, consistent with the two exponents $m_A = 0.24$ and 3.0 for Fig. 2(b). (Note that energy R_{AE} is the square of the AE amplitude.) Reference [10] also reports a spatiotemporal chaotic state that corresponds to the

"edge of peeling picture" for high tape mass $m=0.1$, $I=0.01$, and low pull speeds. However, as experimental AE signals become chaotic as a function of pull velocity (not studied in Ref. [10]), the correct quantity to analyze is the energy dissipated in the form of AE, $R_{AE}(t)$ (an average over the peel front).

Following the embedding technique, we have analyzed the model AE signal $R_{AE}(t)$ and computed the correlation dimensions and Lyapunov spectrum for the entire instability domain. We find stable positive and zero exponents for a range of ϵ_0 values. A plot of the spectrum for $m=0.001$ and $V^s=2.48$ ($\epsilon_0=0.08$) is shown in Fig. 4(b), which gives $D_{ky}=2+0.32/0.77=2.4$ while $\nu=2.2\pm0.02$ [19]. Converged values of ν ranging from 2.2 to 2.7 (D_{ky} in the range 2.4 to 3.0) are seen in the subinterval $1.48\le V^s\le6.48$ of the instability along with stable positive exponents. Similar converged values of ν for $m=0.055$ (ranging from 2.6 to 3.2 with D_{ky} in the range 2.7 to 3.3) are seen in a midrange of V^s. The value of the positive exponent decreases for large V^s.

Several conclusions emerge from the study. First, the presence of chaos in experimental AE signals supported by the model shows that deterministic dynamics is responsible for AE during peeling. Second, the model also provides answers to questions raised by the TSA. For instance, the model shows that while stick slip is controlled by the peel force function, acoustic emission R_{AE} is controlled by the local kinetic energy bursts on the peel front generated during switching between the stuck and peeled states [Fig. 4(a)]. This mechanism provides insight into the transition from burst to continuous type of AE. At low pull velocities, V^s, the number of stuck segments are few, each containing many spatial points [Fig. 4(a)], with only a few large velocity bursts leading to burst type $R_{AE}(t)$. With increasing V^s, the number of stuck segments increases (each containing fewer points) with a large number of small local velocity bursts that

therefore lead to continuous AE signals [similar to Figs. 3(b) and 3(c) of Ref. [10]]. Hence, the decreasing trend of the positive Lyapunov exponent with pull velocity observed in experimental signals can be attributed to peel front breaking up into large number of small stuck-peel segments. Thus, the model provides insight and clarifies the connection between stick slip and the AE process. The work also addresses the general problem of extracting dynamical information from noisy AE signals.

Our study has relevance to time dependent issues of adhesion, in particular, to failure of adhesive joints and composites that are subject to fluctuating loads. Specifically, the analysis suggests that a larger value of the positive Lyapunov exponent (its inverse giving the time scale) implies higher dissipation and hence earlier failure. Thus, using the acoustic emission technique to monitor AE signals in these cases coupled with the estimation of the largest Lyapunov exponent could prove to be useful.

Many of these features are common to the PLC effect. The effect attributed to pinning and unpinning of dislocations from solute atmosphere is clearly a distinct physical process from peeling. Yet, the negative force-velocity relation and the existence of chaotic dynamics in a midrange of drive rates are seen both experiments and a model for the PLC effect as well [8,9,17]. Dynamically, the existence of chaotic dynamics as also the decreasing trend of the positive Lyapunov exponent, seen in both in the PLC effect and peeling, is the result of a reverse forward Hopf bifurcation (HB) (end of the instability) that follows the forward HB (onset) [9]. As a chaotic window is seen in both cases, it is likely that it is a general feature in other stick-slip situations that are limited to a window of drive rates.

[1] N. J. Glassmaker *et al.*, Proc. Natl. Acad. Sci. U.S.A. **104**, 10786 (2007), and references therein.

[2] K. Kendall, *Molecular Adhesion and Its Applications* (Kluwer Academic, New York, 2001).

[3] M. Urbakh *et al.*, Nature (London) **430**, 525 (2004).

[4] B. N. J. Persson, *Sliding Friction: Physical Principles and Applications*, 2nd ed. (Springer, Heidelberg, 2000).

[5] Rumi De, A. Zemel, and S. A. Safran, Nat. Phys. **3**, 655 (2007).

[6] D. Maugis and M. Barquins, in *Adhesion 12*, edited by K. W. Allen (Elsevier, London, 1988), p. 205.

[7] M. Ciccotti, B. Giorgini, D. Villet, and M. Barquins, Int. J. Adhes. Adhes. **24**, 143 (2004); M. Ciccotti, B. Giorgini, and M. Barquins, *ibid.* **18**, 35 (1998).

[8] G. Ananthnakrishna, Phys. Rep. **440**, 113 (2007).

[9] G. Ananthakrishna and M. S. Bharathi, Phys. Rev. E **70**, 026111 (2004).

[10] Rumi De and G. Ananthakrishna, Phys. Rev. Lett. **97**, 165503 (2006).

[11] A. Petri, G. Paparo, A. Vespignani, A. Alippi, and M. Costantini, Phys. Rev. Lett. **73**, 3423 (1994); P. Diodati, F. Marchesoni, and S. Piazza, *ibid.* **67**, 2239 (1991).

[12] M. C. Miguel *et al.*, Nature (London) **410**, 667 (2001).

[13] J. Weiss and D. Marsan, Science **299**, 89 (2003).

[14] P. Bak, C. Tang, and K. Wiesenfeld, Phys. Rev. Lett. **59**, 381 (1987).

[15] P. Grassberger and I. Procaccia, Physica D **9**, 189 (1983).

[16] R. Hegger, H. Kantz, and T. Schreiber, Chaos **9**, 413 (1999).

[17] G. Ananthakrishna, S. J. Noronha, C. Fressengeas, and L. P. Kubin, Phys. Rev. E **60**, 5455 (1999); S. J. Noronha, G. Ananthakrishna, and C. Fressengeas, in *Nonlinear Dynamics, Integrability and Chaos* (Norosa, New Delhi, 2000), p. 235.

[18] J. P. Eckmann, S. O. Kamphorst, D. Ruelle, and S. Ciliberto, Phys. Rev. A **34**, 4971 (1986).

[19] Typical error bars for the positive, zero, and negative exponents are ±0.01, ±0.005, and ±0.05 respectively. D_{ky} values have an error of ±0.05.